AIMS Bioengineering

AIMS Bioengineering, 10(4): 406–420.
DOI: 10.3934/bioeng.2023024
Received: 19 September 2023
Revised: 29 October 2023
Accepted: 31 October 2023
Published: 10 November 2023

http://www.aimspress.com/journal/Bioengineering

Research article

Micro-CT evaluation of bone grow concept of an implant with microstructured backtaper crestally and sub-crestally placed. Preliminary study in New Zealand rabbits tibia at one month

José Luis Calvo-Guirado[1,*], Marta Belén Cabo-Pastor[2], Félix de Carlos-Villafranca[3], Nuria García-Carrillo[4], Manuel Fernández-Domínguez[5] and Francisco Martínez Martínez[6]

[1] Health Sciences Faculty, Universidad Autónoma de Chile, Santiago de Chile 7500912, Chile; Private Practice Murcia, Spain
[2] Advanced Prosthodontics, Dentistry Department, Universidad C.E.U. Cardenal Herrera, 46001 Valencia, Spain
[3] Department of Orthodontics, Faculty of Medicine, University of Oviedo, 33001 Asturias, Spain
[4] Department of Veterinary, University of Murcia, 30007 Murcia, Spain
[5] Director of Dentistry Degree, Universidad Camilo José Cela, 28001 Madrid, Spain
[6] Department of Traumatology, Hospital Clínico Universitario Virgen de la Arrixaca, ctra. Madrid-Cartagena s/n, 30120, El Palmar, Murcia, Spain

*** Correspondence:** Email: joseluis.calvoguirado@gmail.com.

Abstract: The primary purpose of this study was to determine the accuracy of micro-computed tomography (micro-CT) as a novel tool for the 3D analysis of bone density around dental implants in tibia rabbits. Six male New Zealand rabbits were used in our evaluation. One Copa SKY® (Bredent Medical GmbH & Co. K.G.) with a 3.5 mm diameter by 8.0 mm in length was placed within 12 tibia rabbits divided into two experimental groups: Group A (crestal placement) and Group B (sub-crestal placement). The animals were sacrificed at four weeks. Micro-CT evaluations showed a high amount of bone around all implants in the tibia rabbit bone. There was an increased formation of bone around the Copa SKY implants, mainly in the implants that were placed crestally. The most frequent density found in most implants was a medullary bone formation surrounding the implant; the density three (D3) was the most common type in all implants. The 3D model analysis revealed a mean bone volume (B.V.) of 31.24 ± 1.24% in crestal implants compared with the 43.12 ± 0.43% in sub-crestal implants. The mean actual contact implant to bone (B.I.C.) in the sub-crestal group was 51.76 ± 0.86%,

compared to the 42.63 ± 0.75% in the crestal group. Compared to crestal implants, the Copa Sky implant placed sub-crestally allows for the formation of bone on top of the neck, thereby stimulating bone growth in tibia rabbits.

Keywords: Copa Sky; crestal implants; subcrestal implants; tibia dental implants

1. Introduction

Diagnostic images have significantly contributed to the advancement of biomedicine and the acceleration of diagnostic processes and treatment plans, thus improving the patients' quality of life [1]. The development of various capture techniques has required advances in their characterization and processing, thus consolidating a specific discipline in current medicinal practices. Digital image processing and analyses have included the development of various extraction methods of information by different types of programs that integrate digital information and develop a diagnosis and treatment plan [2]. Compared with other types of topographies, the use of microcomputed tomography (micro-CT) is the best method for the qualitative and morphological evaluation of bone and stiff structures within the body [3]. Therefore, the pictures acquired across computerized microtomography result from a volumetric decomposition of the body into either voxels or units. Each extracted voxel expresses the attenuation coefficients, also known as "raw data". The raw data volumetric group is mathematically reconstructed, thereby obtaining a pixelated image [4,5]. All data obtained are strongly related between the size and number of voxels, the resolution of the image acquisition, and the volumetric reconstruction of the object in a pixelated and multiplanar image associated with the loss of the data; for a definitive evaluation, they are introduced as errors within the system [5]. Related errors in radiographic interpretation alerted the scientists to errors in the radiographic interpretation when limited exclusively by the pixel value [6]. In order to reduce errors and false negatives, two programs were determined, such as a computer-aided detection (CAD) program, which is software that digitally analyzes all the images and estimates the expectation of distortion located on algorithms [7–11]. New strategies have been introduced to implant new biomaterials and implants in favor of bone formation, vascularization, and tissue stability [12]. Scarano et Al. confirmed that the most efficient approach for accelerating early osteogenesis and improving the bioactivity of titanium implant surfaces involves the use of collagen type I on the implant surface and could be clinically advantageous for shortening the implant healing period [13].

Micro-CT is a predominant technique used to improve imaging techniques, such as the evaluation of medullary and cortical bones, as well as evaluating bone formation and resorption in both 2D and 3D [14,15]. Parrilla-Almansa and Cols presented a study combining a radiological study and a mathematical analysis of raw data obtained by micro CT, thereby adapting these analyses to the quality, density, and location of the implanted biomaterial in the evolution of its maturation over time. Because micro-CT is a non-aggressive technique, these data can be transported to other areas of radiology related to dental implants, thereby allowing us to see the bone's characteristics that form within the dimension of the implants [16].

2. Materials and methods

The preliminary evaluation was performed as follows. Day zero equates to the day of the surgery, in which the crestal and subcrestal implants are placed within the tibias of New Zealand white rabbits. After four weeks, the animals are sacrificed and the micro-CTs are evaluated.

2.1. Animals

This study used six male New Zealand white rabbits in good shape (provided by the Animal Center, Murcia University), all weighing 2.59 ± 0.12 kg. The Bioethical University of Murcia Committee, Spain, authorized the research protocol number (A1320140404-15/04/2014), which followed guidelines validated by the Council on 22 September 2010 (2010/63/E.U.). Animals were quarantined and kept in rabbit cages, receiving appropriate veterinary care. Rabbits were provisioned with a granulated diet, watered ad libitum, and housed in individual cages. Cages were maintained at an ambient temperature of 21 ± 05 °C, with alternating 12 h periods of natural light and darkness. All animals were fasted overnight prior to the surgical operations. In our study, we chose a rabbit tibia model to evaluate the potential ability of coating surfaces to enhance bone formation in the presence of large medullary spaces.

2.2. Implants

Twelve titanium implants which were sandblasted and acid etched (Copa SKY; Bredent Medical GmbH & Co. K.G.), with a 3.5 mm diameter by 8.0 mm in length, were placed within the tibias of 12 rabbits (Figure 1). The surface of the Copa SKY titanium implants has three morphologic dimensions (Rugosity Ra ~2.2 μm). The backtaper is only microstructured by edging (Rugosity Ra ~0,36 μm). The platform around the abutments is machined (Rugosity Ra ~0,07 μm). Fifteen minutes before general anesthesia, the animals received an I. M. injection of an anxiolytic (0.5–1 mg/kg acepromazine maleate) (Calmo-Neosan, Madrid, Spain). The rabbits were anesthetized with an intramuscular injection of tiletamine/zolazepam (15 mg/kg) (Zoletil 50, Virbac, Madrid, Spain) and xylazine (5 mg/kg) (Rompun, Bayer, Leverkusen, Germany). Before surgery, the skin over the proximal tibia was shaven and washed with betadine (Meda Manufacturing, Burdeos, France). Ketamine hydrochloride (Ketolar; Pfizer, Madrid, Spain) was administered as an anesthetic at 50 mg/kg alongside amoxicillin as an I.M. pre-operative antibiotic (Pfizer, Barcelona, Spain). Additionally, 3 mL of 2% lidocaine (Normon, Barcelona, Spain) was administered by an I.M. injection in the surgical area of each leg, alongside 0.01 mg/mL of adrenaline.

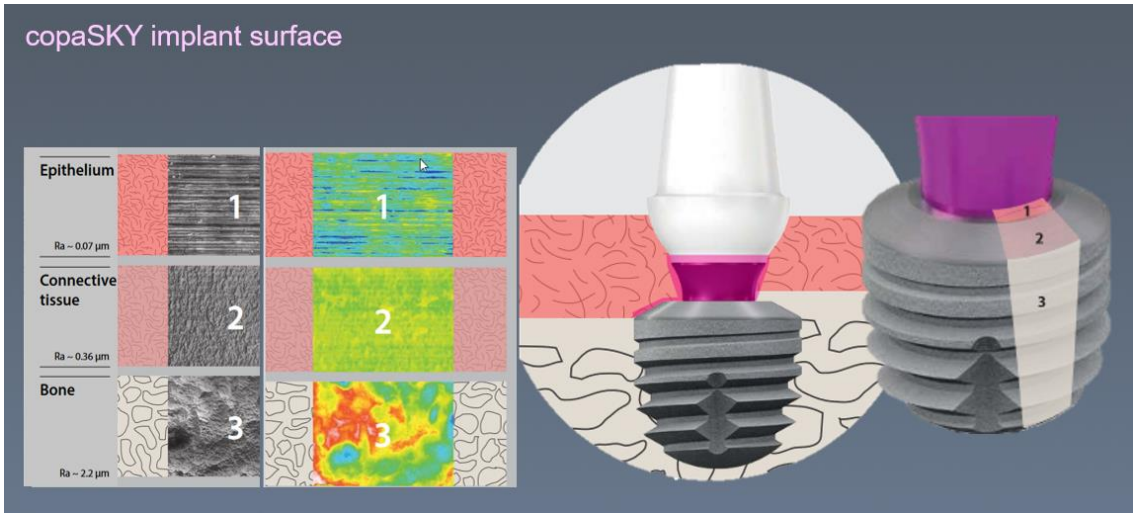

Figure 1. CopaSKY implant surface.

2.2.1. Study groups

The study animals were split up into two groups (n = 6) according to the position within the tibia: Copa SKY crestal (Group A) and Copa SKY sub-crestal (Group B). All rabbit tibias were used for scanning with Micro-CT (Figure 2).

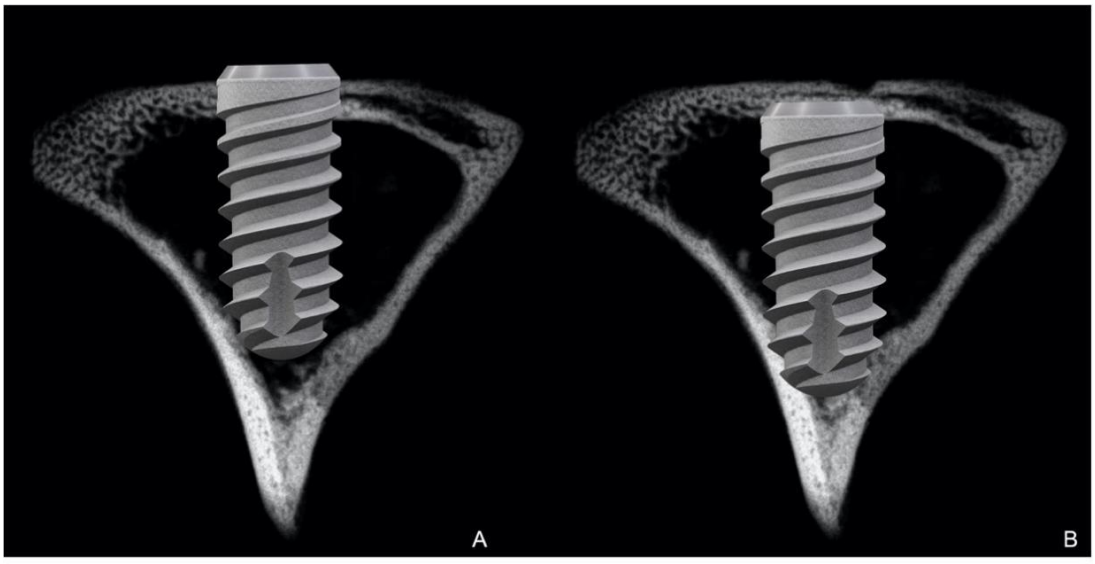

Figure 2. CopaSKY implant placement in tibia rabbits.

2.2.2. Surgical procedure

The tibial approach was performed in the internal area of each tibia, 7 millimeters below the anterior tibial tuberosity. A linear 20-millimeter cut was performed at the internal area of each rabbit tibia. A full-thickness flap was elevated to the uncovered bone area, utilizing the tibial plateau as a

reference point. Consequently, the perforation of the cortical bone was carried with implant drills at approximately 3.5/4.0 mm in diameter and 8 mm in length (Bredent Medical GmbH & Co. K.G.) under profuse irrigation, and each tibia received one implant (Figure 3A,B). The implant diameter and length were the same for all implant groups (3.5 mm diameter and 8.5 mm length). The study was randomized, placing one implant in each tibia to protect and prevent bone fracture (http://www.randomization.com).

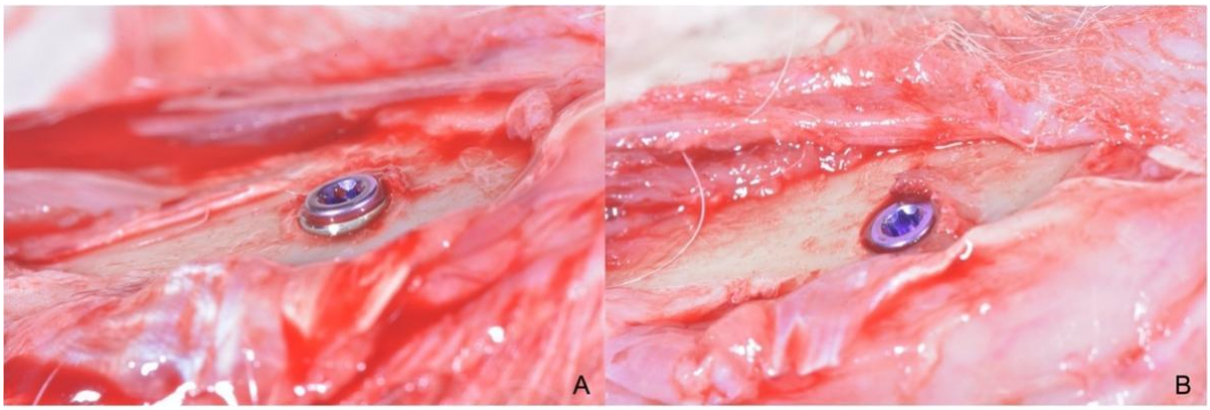

Figure 3. (A) Group A, copaSKY Crestal; (B) Group B, copaSKY sub-crestal 2 mm.

The Copa SKY implants were crestally exposed only 1 mm over the cortical bone; for the other group, the Copa SKY implants were placed 1mm sub-crestally (Figure 3A,B). The mucoperiosteal flaps were repositioned and sutured with 3-0 silk (Laboratories Lorca Marin. Lorca, Murcia, Spain). Penilicilin (0.1 mL/kg intramuscularly) was administrated at the end of the surgery, as well as 0.05 mg/kg ibuprofen subcutaneously every 12 h after the operation, for a total of three days.

2.2.3. Micro-CT sample preparation and analyses

All biopsies were mended in 10% buffered formalin and sent to the complex tissue laboratory of the Biomaterials Clinical-Histological Research Association (BioCRA). The specimens were processed for histology, de-hydrated, and then stuck in methacrylate resin. After polymerization, the models were observed with a lofty-resolution micro CT system using an Albira trimodal preclinical scanner (Bruker®, Massachusetts, U.S.A.); an image was obtained with a resolution of less than 0.05 mm and was reconstructed in 3D (Figure 4). The specimens were scanned in high resolution with an x-, y-, and z-axis resolution of approximately 20 μm. The voxel size was 15 × 15 × 15 μm^3. The scanning time for each specimen was approximately 12 h. A morphologic analysis was performed by an accurate observation of the 2D sections and the 3D reconstructions. The morphometric analysis enabled the calculation of actual contact implant to bone (B.I.C.), expected implant-cone contact (E.B.C.), bone volume (B.V.), and standard morphometric indices. Bone-to-implant contact is a concept calculating the amount of the implant surface directly attached to mineralized bone without soft tissue interposition. B.I.C. was calculated by micro-CT (automatic measurement of bone density). The E.B.C. is a virtual value, which was calculated by superimposing the implant thread profile over the bone image at various distances from the actual implant site (1.0, 1.25, or 1.5 mm), followed by counting the quantity of bone in contact with the implant surface, as described by other authors [17,18].

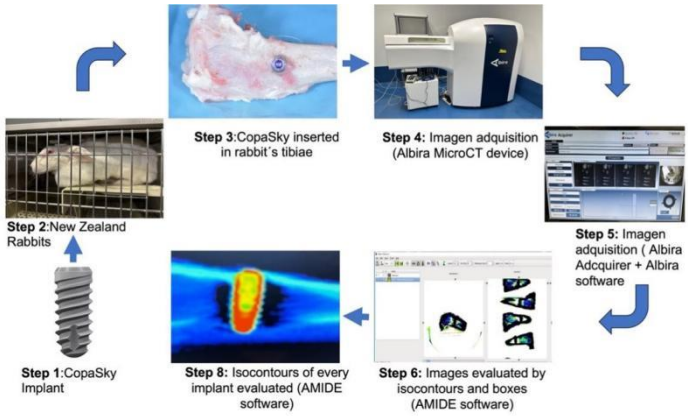

Figure 4. Diagram of animal study using Micro C.T..

Measurements were calculated using a medical imaging data examiner (Amide, UCLA University, LA, U.S.A.). A global description of all statistical values was made, including the mean, standard deviation, median, minimum value, maximum value, size of the volume of interest (VOI) in mm^3, voxel fraction, and total voxels. An analysis of both the biomaterials and the biopsies was performed, thereby calculating the percentages of Hounsfield units (HU) that characterized the samples by determining the predefined composition, type of density, and volumes and creating individual isocontours following the subjective classification of bone quality, as described by Misch in four types of bone density differentiation: D4 (200–400 HU), D3 (450–800 HU), D2 (800–1100 HU) and D1 (>1200 HU). The bone volume in this area was expressed as a percentage of the total volume of the region of interest (ROI) as a 5 mm square area in the middle of the implant covering the mesial and distal inner and outer areas of the threads (Figure 5). The hard tissue cores used were scanned by an Albira Micro-Ct, thereby obtaining an image with a resolution of less than 0.05 mm and was reconstructed in 3D (Figures 5 and 6). The acquisition parameters are summarized in Table 1.

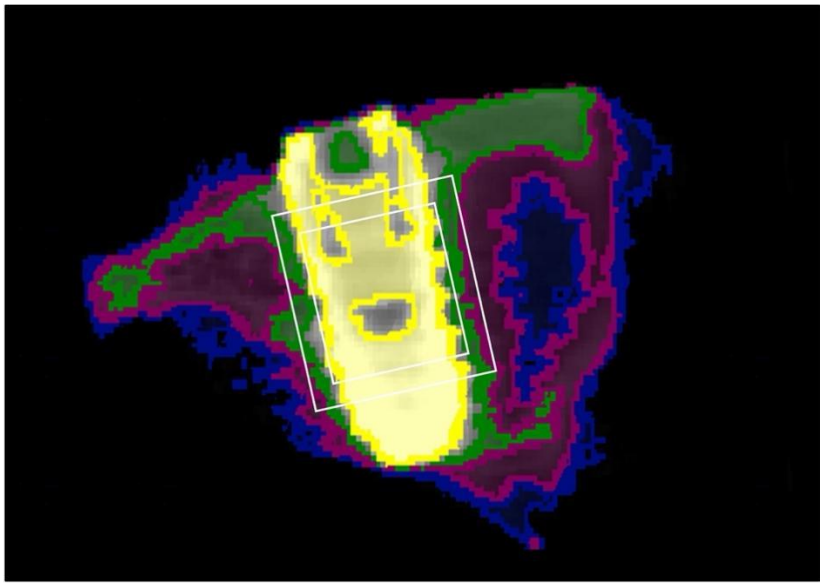

Figure 5. Region of interest (R.O.I.).

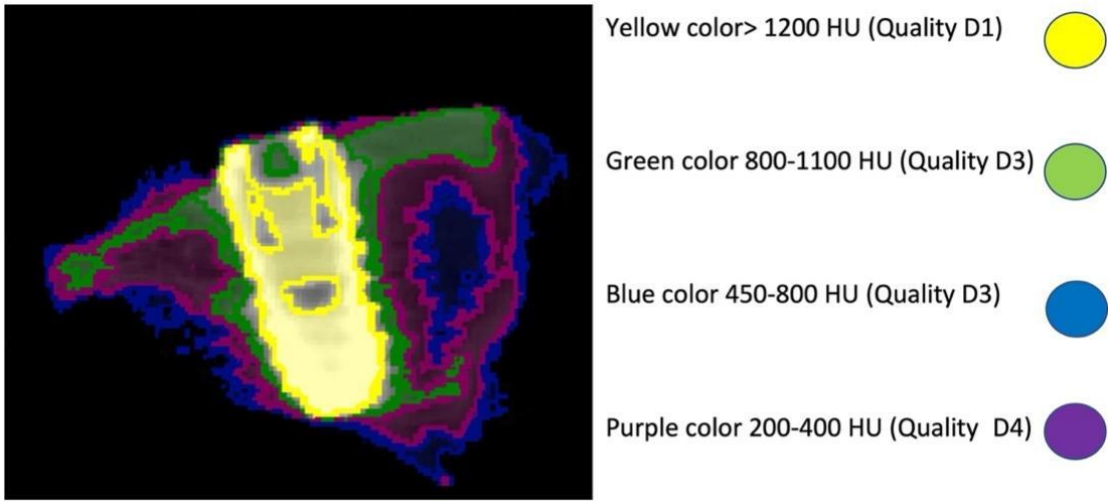

Figure 6. Bone density classified in colors.

In this study, 200 HU was the minimum density value selected for the D4 density. The results indicated the imparted dose at the surface level of the current (0.3 or 0.4 mA) and the voltage (44 kV) for best, excellent, and standard image acquisition modalities [19].

The measurement method developed is presented as follows.

Table 1. MicroCT acquisition parameters (Own design for each biomaterial).

Voltage	44 kV
Intensity	0.3 mA
Dosis	0.4 mA
Voxels size	0.05 mm
High Resolution	600 projections
Digital flat panel	2401 × 2401 pixels
Field of view	80 × 80 mm
Reconstructed	Filtered backprojection algorithm (FBP)

Two quantitative parameters were estimated (Figure 3):

1-BIC: The implant bone contact around and along the entire length of the implant is measured, starting from the neck to the tip of the implant.

2- Percentage of peri-implant bone area (B.V.): The amount of bone mass around an implant is analyzed by a rectangular measurement ROI in the middle of the implant. B.V. measurements are based on quantifying the specified loose tissue in the ROI around all implants. All measurements were performed on both sides of the implant.

2.2.4. Statistical analysis

All statistical analysis was performed using the GraphPad Prism 6 software (GraphPad Software, Inc., San Diego, CA, USA). The Student *t*-Test was used to determine the statistical significance between the two groups of crestal and sub-crestal placements. A power analysis of 0.9 is connected with a 90% detection level. The level of significance for the analysis was set at $p \leq 0.05$.

3. Results

All wounds were cured without complications, and the animals survived at four weeks of healing. The dental implants were retrieved after four weeks of healing. Micro-CT evaluations showed a high amount of bone around all implants placed within the tibias of the rabbits. Bone formation significantly increased around the Copa SKY implants, mainly in the implants placed sub-crestally due to the position and surface of them. The most frequent density found among the implants was a medullary bone formation that surrounded the implant; the D3 (less cortical bone with high medullar bone) density was the most common type in all implants (Figure 6). This kind of bone implant stimulates bone formation because of an increase in calcium deposition onto the bloody bone marrow. One can understand the micro-CT by utilizing colors to classify the bone densities, as we can see in Figure 6.

3.1. Micro-CT findings

One of the most critical findings in this preliminary study of the rabbit tibias was that most of the implants placed crestally to the bone were situated above the shoulder of the bone. The implants were placed in such a way that the crestal of the bone covers not only the shoulder, but also the closing cap of the implant. The micro-CT examination exhibited excellent osseointegration among all the implants placed at crestal and sub-crestal locations. The 3D model analysis revealed a mean B.V. of 31.24 ± 1.24% in crestal implants compared with the 43.12 ± 0.43% in sub-crestal implants (Table 2). The mean B.I.C. in the sub-crestal group was 51.76 ± 0.86%, as compared to 42.63 ± 0.75% in the crestal group (Figure 7). The sub-crestal implants showed a significantly greater volume than the crestal implants. The bone-to-implant contact was significantly higher in the sub-crestal group compared to the crestal group (Figure 8).

Table 2. MicroCT measurements of bone density classified in colors.

Bone density	Hounsfield units	Color
D1	>1200	Yellow
D2	800–1100	Green
D3	450–800	Blue
D4	200–400	Purple

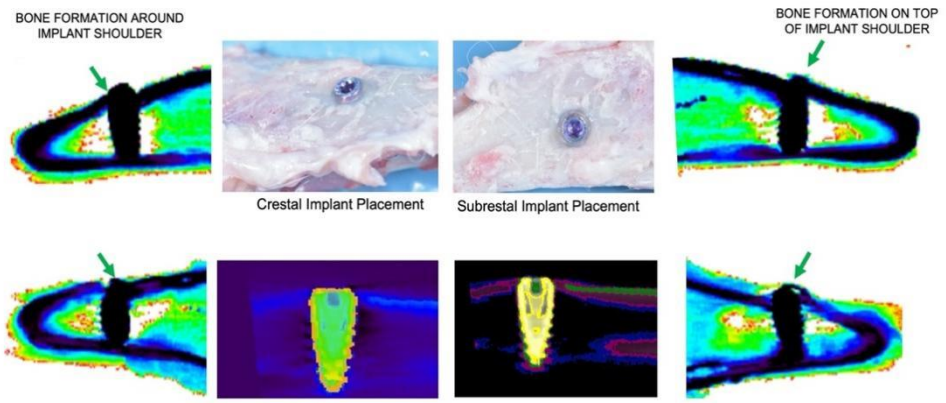

Figure 7. Bone formation on top of all CopaSky implants shoulders.

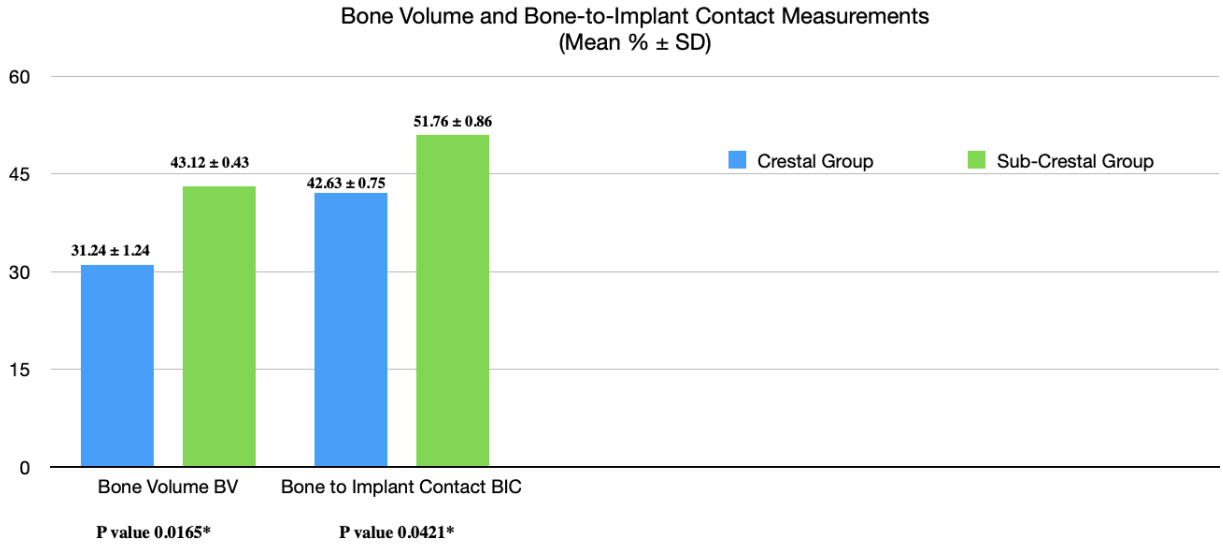

Figure 8. Bone volume and bone-to-implant contact measurements (Mean% ± SD).

4. Discussion

Numerous companies have developed an implant surface that improves the bonding effect to the bone due to the length of the threads and the connection on the coronal surface. The design of a smooth-surfaced implant in the neck allows the bone to grow over the neck, thus avoiding crestal bone resorption [20]. This research was performed by analyzing the complete osseointegration of dental implants by a micro-CT assessment, which reveals improved osseointegration in the implants placed sub-crestally. The micro-CT scanner was designed to evaluate small animals based on pixelated detectors, which is widely used to evaluate the utilization of different implants and biomaterials in small animals [21]. These previous studies coincide with the findings in our experimental animals, thus allowing us to evaluate the bone quality found in bone grafts and dental implants. For example, Al Deeb and coworkers demonstrated significantly improved BIC and BV percentages for TM

implants using a micro-CT evaluation [22–26]. Other studies related to micro-CT can also demonstrate the disruption of osseointegration in heavy smokers due to nicotine, thereby reducing the bone volume acting on super-hydrofilic implant surfaces [27]. These observations made in the animal studies coincide with previous clinical studies by other authors. In these studies, the bone response that occurs in the animals coincide with the attribution of the increase in the B.I.C. because rabbit tibias ensure the placement of the implants in a bi-cortical manner [28,29]. These animal models offer the opportunity for observing implant stability and histological observations, thereby allowing researchers to measure the BIC and BV with different surface coatings [30]. One of the mechanisms that can explain this integration phenomenon related to the damage produced in the tibia and the heat generated when we place the implant has been published in previous investigations [31–33]. A delayed implant placement may be a more effective method of achieving osseointegration, thus leaving approximately 14 days after cavity preparation with the implant burs. Futami et al. demonstrated that the micro space that exists between the surface implant and hard tissue allows for the dissemination of osteogenic cells that come from the bone spaces to the implant surface [34]. The limitations of this study are due to the animal model used. Other species such as rodent primates allow for the rapid turnover of changes that occur in the bone much quicker than in humans [35,36]. The placement of implants in healed bone or immediate implants for extraction is vital to their neck, which can either stimulate or reabsorb the bone, thus allowing for an adequate establishment of the biological width [37–42]. Many of our studies have been related to the immediate post-extraction of dental implants placed either 1 or 2 mm underneath the bone crest, especially in the experimental animals who underwent 12 weeks of healing, in which the reabsorption of these crestal walls of bundle bone does not independently influence the implant position [43]. Some studies place the implants 1 mm under the bone walls and reduce the platform immediately, which act in a gap reduction and biologic width protection over the neck of the implant, thereby serving as an umbrella for the bone surrounding the implant [43–48]. Many authors describe that the position of the implant does not influence the changes that occur in the bundle bone; however, these changes do occur, and have a significant influence on the soft tissue, greatly depending on the depth of implant placement and the thickness and type of gum of abutment that is placed on the implant [49]. The micro-CT application can demonstrate mineral bone density formation close to the implants treated with different surfaces, thereby improving the optimal integration of implants in the rabbits' long bones [50–52]. The use of micro-CT imaging techniques and immunohistochemistry are excellent tools for this objective, since they both enable the quantitative assessment of bone microarchitecture and intercellular interaction [53]. Recent studies demonstrated that collagen type I and augmented wettability accelerates early osteogenesis and improves the bioactivity, such as Autologous Platelet Liquid (APL) on titanium implant surfaces [54]. Other authors suggest that implant surface modifications can be a new alternative to the administration of systemic drugs such as calcium-doping and fibrinogen-conditioning, thus combining local antibiotic therapy with a surface treatment with a proven efficacy, improving the integration of the titanium implant to the bone [54,55]. However, other authors found that placing implants at the crestal level increased the implant-bone contact, especially in cylindrical implants [49,56]. Our results demonstrated that micro-CT is a valuable method for the 3D assessment of bone skeleton around implants [57]. The micro-TC PET/SPECT/CT is proposed to evaluate small animals, thereby obtaining high-quality images for studies, decreasing the cost, the number of animals, and the 3R [20]. Micro-CT is a fundamental diagnostic tool after the implantation of biomaterials, allowing us to assess the density of the bone that forms around and above the head of the implants.

5. Conclusions

Sub-crestal implants allow bone formation on the neck, thereby stimulating bone growth compared to crestal implants. The crestal position endures bone to grow around the neck of the implant, unlike sub-crestal implants, where the bone grows above the neck and the cover screw of the implant. This is mainly due to the sub-crestal position stimulating the surrounding tissues, thereby increasing the formation of collagen and neo-angiogenesis on the neck of the implant. In addition, this increases implant-bone contact and the bone volume that adheres to the implant, thus favoring healing and osseointegration.

Use of AI tools declaration

The authors declare they have not used Artificial Intelligence (AI) tools in the creation of this article.

Conflict of interest

The authors declare no conflict of interest

Author Contributions:

Conceptualization: José Luis Calvo-Guirado, Nuria Garía-Carrillo; data curation: Marta Belen Cabo-Pastor; formal analysis: Félix de Carlos-Villafranca; funding acquisition: José Luis Calvo-Guirado, Manuel Fernández-Domínguez, Francisco Martínez Martínez, investigation: José Luis Calvo-Guirado, Marta Belen Cabo-Pastor; methodology: Nuria Garía-Carrillo, Félix de Carlos-Villafranca; project administration: Francisco Martínez Martínez, José Luis Calvo-Guirado; resources: José Luis Calvo-Guirado; software: Félix de Carlos-Villafranca; supervision: José Luis Calvo-Guirado; validation: Marta Belen Cabo-Pastor; visualization: José Luis Calvo-Guirado; writing—original draft preparation: José Luis Calvo-Guirado; writing—review and editing: José Luis Calvo-Guirado, Félix de Carlos-Villafranca, Marta Belen Cabo-Pastor, Manuel Fernández-Domínguez.

References

1. Lehmann TM, Meinzer HP, Tolxdorff T (2004) Advances in biomedical image analysis. *Methods Inf Med* 43: 308–314. https://doi.org/10.1055/s-0038-1633873
2. Handels H, Mersmann S, Palm C, et al. (2013) Viewpoints on medical image processing: from science to application. *Curr Med Imaging* 9: 79–88. https://doi.org/10.2174/1573405611309020002
3. Bouxsein ML, Boyd SK, Christiansen BA, et al. (2010) Guidelines for assessment of bone microstructure in rodents using micro–computed tomography. *J Bone Miner Res* 25: 1468–1486. https://doi.org/10.1002/jbmr.141
4. Höhne KH, Bomans M, Pommert A, et al. (1990) 3D visualization of tomographic volume data using the generalized voxel model. *Vis Comput* 6: 28–36. https://doi.org/10.1007/BF01902627

5. Beister M, Kolditz D, Kalender WA (2012) Iterative reconstruction methods in X-ray CT. *Phys Med* 28: 94–108. https://doi.org/10.1016/j.ejmp.2012.01.003
6. Garland LH (1994) On the scientific evaluation of diagnostic procedures: Presidential address thirty-fourth annual meeting of the radiological society of North America. *Radiology* 19452: 309–328. https://doi.org/10.1148/52.3.309
7. Berlin L (2014) Radiologic errors, past, present, and future. *Diagnosis* 1: 79–84. https://doi.org/10.1515/dx-2013-0012
8. Bruno MA, Walker EA, Abujudeh HH (2015) Understanding and confronting our mistakes: The epidemiology of error in radiology and strategies for error reduction. *Radiographic* 35: 1668–1676. https://doi.org/10.1148/rg.2015150023
9. Waite S, Scott J, Gale B, et al. (2017) Interpretive error in radiology. *Am J Roentgenol* 208: 739–749. https://doi.org/10.2214/AJR.16.16963
10. Castellino RA (2005) Computer aided detection (CAD): an overview. *Cancer Imaging* 5: 17–19. https://doi.org/10.1102/1470-7330.2005.0018
11. Doi K (2007) Computer-aided diagnosis in medical imaging: historica review, current status and future potential. *Comput Med Imaging Graph* 31: 198–211. https://doi.org/10.1016/j.compmedimag.2007.02.002
12. Parrilla-Almansa A, García-Carrillo N, Ros-Tárraga P (2018) Demineralized bone matrix coating Si-Ca-P ceramic does not improve the osseointegration of the scaffold. *Materials* 11: 1580. https://doi.org/10.3390/ma11091580
13. Scarano A, Lorusso F, Orsini T, et al. (2019) Biomimetic surfaces coated with covalently immobilized collagen type I: An X-Ray photoelectron spectroscopy, atomic force microscopy, Micro-CT and histomorphometrical study in rabbits. *Int J Mol Sci* 20: 724. https://doi.org/10.3390/ijms20030724
14. Martinez IM, Velasquez PA, de Aza PN (2010) Synthesis and stability of tricalcium phosphate doped with dicalcium silicate in the system $Ca_3(PO_4)_2$–Ca_2SiO_4. *Mater Charact* 61: 761–767. https://doi.org/10.1016/j.matchar.2010.04.010
15. Kim SY, Kim YK, Park YH, et al. (2017) Evaluation of the healing potential of demineralized dentin matrix fixed with recombinant human bone: morphogenetic protein-2 in bone grafts. *Materials* 10: 1049. https://doi.org/10.3390/ma10091049
16. Parrilla-Almansa A, González-Bermúdez CA, Sánchez-Sánchez S, et al. (2019) Intraosteal behavior of porous scaffolds: The mCT raw-data snalysis as a tool for better understanding. *Symmetry* 11: 532. https://doi.org/10.3390/sym11040532
17. Trisi P, Lazzara R, Rao W, et al. (2002) Bone-implant contact and bone quality: Evaluation of expected and actual bone contact on machined and Osseotite implant surfaces. *Int J Periodontics Restorative Dent* 22: 535–545. PMID: 12516825
18. Rebaudi A, Laffi N, Benedicenti S, et al. (2011) Microcomputed tomographic analysis of bone reaction at insertion of orthodontic mini-implants in sheep. *Int J Oral Maxillofac Implants* 26: 1233–1240. PMID: 22167428.
19. Rueda AN, Ruiz-Trejo C, López-Pineda E, et al. (2021) Dosimetric evaluation in micro-CT studies used in preclinical molecular imaging. *Appl Sci* 11: 7930. https://doi.org/10.3390/app11177930

20. Calvo-Guirado JL, Ortiz-Ruiz AJ, Negri B, et al. (2010) Histological and histomorphometric evaluation of immediate implant placement on a dog model with a new implant surface treatment. *Clin Oral Implants Res* 21: 308–315. https://doi.org/10.1111/j.1600-0501.2009.01841.x
21. Sánchez F, Orero A, Soriano A, et al. (2013) ALBIRA: a small animal PET/SPECT/CT imaging system. *Med Phys* 40: 051906. https://doi.org/10.1118/1.4800798
22. Calvo-Guirado JL, Nuria García Carrillo, Félix de Carlos-Villafranca, et al. (2022) A micro-CT evaluation of bone density around two different types of surfaces on one-piece fixo implants with early loading-an experimental study in dogs at 3 months. *AIMS Bioeng* 9: 383–399. https://doi.org/10.3934/bioeng.2022028
23. Calvo-Guirado JL, Carlos-Villafranca Fd, Garcés-Villalá M, et al. (2022) X-ray micro-computed tomography characterization of autologous teeth particle used in postextraction sites for bone regeneration. An experimental study in dogs. *Indian J Dent Sci* 14: 58–67. https://doi.org/10.4103/ijds.ijds_138_21
24. Calvo-Guirado JL, Carlos-Villafranca FD, Garcés-Villalá MA, et al. (2022) How much disinfected ground tooth do we need to fill an empty alveolus after extraction? Experimental in vitro study. *Indian J Dent Sci* 14: 171–177. https://doi.org/10.4103/ijds.ijds_24_22
25. Al Deeb M, Aldosari AAF, Anil S (2023) Osseointegration of tantalum trabecular metal in titanium dental implants: histological and micro-CT study. *J Funct Biomater* 14: 355. https://doi.org/10.3390/jfb14070355
26. Anil S, Cuijpers VMJI, Preethanath RS, et al. (2013) Osseointegration of oral implants after delayed placement in rabbits: a microcomputed tomography and histomorphometric study. *Int J Oral Max Impl* 28: 1506–1511. https://doi.org/10.11607/jomi.3133
27. Pinotti FE, Aroni MAT, Oliveira GJPL, et al. (2023) Osseointegration of implants with superhydrophilic surfaces in rats with high serum levels of nicotine. *Braz Dent J* 34: 105–112. https://doi.org/10.1590/0103-6440202305096
28. Kunnekel AT, Dudani MT, Nair CK, et al. (2011) Comparison of delayed implant placement vs immediate implant placement using resonance frequency analysis: a pilot study on rabbits. *J Oral Implantol* 37: 543–548. https://doi.org/10.1563/AAID-JOI-D-10-00022.1
29. Bansal J, Kedige S, Bansal A, et al. (2012) A relaxed implant bed: Implants placed after two weeks of osteotomy with immediate loading: a one year clinical trial. *J Oral Implantol* 38: 155–164. https://doi.org/10.1563/AAID-JOI-D-10-00036
30. López-Valverde N, López-Valverde A, Cortés M P, et al. (2022) Bone quantification around chitosan-coated titanium dental implants: A preliminary study by micro-CT analysis in jaw of a canine model. *Front Bioeng Biotechnol* 10: 858786. https://doi.org/10.3389/fbioe.2022.858786
31. Berglundh T, Abrahamsson I, Lang NP, et al. (2003) De novo alveolar bone formation adjacent to endosseous implants. *Clin Oral Implants Res* 14: 251–262. https://doi.org/10.1034/j.1600-0501.2003.00972.x
32. Franchi M, Fini M, Martini D, et al. (2005) Biological fixation of endosseous implants. *Micron* 36: 665–671. https://doi.org/10.1016/j.micron.2005.05.010
33. Calvo-Guirado JL, Delgado-Peña J, Maté-Sánchez JE, et al. (2015) Novel hybrid drilling protocol: evaluation for the implant healing-thermal changes, crestal bone loss, and bone-to-implant contact. *Clin Oral Implants Res* 26: 753–760. https://doi.org/10.1111/clr.12341

34. Futami T, Fujii N, Ohnishi H, et al. (2000) Tissue response to titanium implants in the rat maxilla: Ultrastructural and histochemical observations of the bone-titanium interface. *J Periodontol* 71: 287–298. https://doi.org/10.1902/jop.2000.71.2.287
35. Castaneda S, Largo R, Calvo E, et al. (2006) Bone mineral measurements of subchondral and trabecular bone in healthy and osteoporotic rabbits. *Skeletal Radiol* 35: 34–41. https://doi.org/10.1007/s00256-005-0022-z
36. Gilsanz V, Roe TF, Gibbens DT, et al. (1988) Effect of sex steroids on peak bone density of growing rabbits. *Am J Physiol* 255: E416–E421. https://doi.org/10.1152/ajpendo.1988.255.4.E416
37. Calvo-Guirado JL, Aguilar-Salvatierra A, Gomez-Moreno G, et al. (2014) Histological, radiological and histomorphometric evaluation of immediate vs. non-immediate loading of a zirconia implant with surface treatment in a dog model. *Clin Oral Implants Res* 25: 826–830. https://doi.org/10.1111/clr.12145
38. Rodríguez-Ciurana X, Vela-Nebot X, Segala-Torres M, et al. (2009) The effect of interimplant distance on the height of the interimplant bone crest when using platform-switched implants. *Int J Periodont Rest* 29: 141–151. PMID: 19408476.
39. Romanos GE, Delgado-Ruiz RA, Nicolas-Silvente AI (2020) Volumetric changes in morse taper connections after implant placement in dense bone. In-vitro study. *Materials* 13: 2306. https://doi.org/10.3390/ma13102306
40. Delgado-Ruiz RA, Calvo-Guirado JL, Abboud M, et al. (2015) Connective tissue characteristics around healing abutments of different geometries: new methodological technique under circularly polarized light. *Clin Implant Dent Relat Res* 17: 667–680. https://doi.org/10.1111/cid.12161
41. Negri B, Calvo Guirado JL, Maté Sánchez de Val JE, et al. (2014) Peri-implant tissue reactions to immediate nonocclusal loaded implants with different collar design: an experimental study in dogs. *Clin Oral Implants Res* 25: 54–63. https://doi.org/10.1111/clr.12047
42. Calvo-Guirado JL, Boquete-Castro A, Negri B, et al. (2014) Crestal bone reactions to immediate implants placed at different levels in relation to crestal bone. A pilot study in Foxhound dogs. *Clin Oral Implants Res* 25: 344–351. https://doi.org/10.1111/clr.12110
43. Sotto-Maior BS, Lima Cde A, Senna PM, et al. (2014) Biomechanical evaluation of subcrestal dental implants with different bone anchorages. *Braz Oral Res* 28: 1–7. https://doi.org/10.1590/1807-3107BOR-2014.vol28.0023
44. Calvo-Guirado JL, López-López PJ, Mate Sanchez JE, et al. (2014) Crestal bone loss related to immediate implants in crestal and subcrestal position: a pilot study in dogs. *Clin Oral Implants Res* 25: 1286–1294. https://doi.org/10.1111/clr.12267
45. Calvo-Guirado JL, Delgado Ruiz RA, Ramírez-Fernández MP, et al. (2016) Histological and histomorphometric analyses of narrow implants, crestal and subcrestally placed in severe alveolar atrophy: a study in foxhound dogs. *Clin Oral Implants Res* 27: 497–504. https://doi.org/10.1111/clr.12569
46. Sánchez-Siles M, Muñoz-Cámara D, Salazar-Sánchez N, et al. (2018) Crestal bone loss around submerged and non-submerged implants during the osseointegration phase with different healing abutment designs: a randomized prospective clinical study. *Clin Oral Implants Res* 29: 808–812. https://doi.org/10.1111/clr.12981

47. de Siqueira RAC, Savaget Gonçalves Junior R, Dos Santos PGF, et al. (2020) Effect of different implant placement depths on crestal bone levels and soft tissue behavior: a 5-year randomized clinical trial. *Clin Oral Implants Res* 31: 282–293. https://doi.org/10.1111/clr.13569
48. de Siqueira RAC, Fontão FNGK, Sartori IAM, et al. (2017) Effect of different implant placement depths on crestal bone levels and soft tissue behavior: a randomized clinical trial. *Clin Oral Implants Res* 28: 1227–1233. https://doi.org/10.1111/clr.12946
49. Fernández-Domínguez M, Ortega-Asensio V, Fuentes Numancia E, et al. (2019) Can the macrogeometry of dental implants influence guided bone regeneration in buccal bone defects? Histomorphometric and biomechanical analysis in beagle dogs. *J Clin Med* 8: 618. https://doi.org/10.3390/jcm8050618
50. Yu YJ, Zhu WQ, Xu LN et al. (2019) Osseointegration of titanium dental implant under fluoride exposure in rabbits: Micro-CT and histomorphometry study. *Clin Oral Implants Res* 30: 1038–1048. https://doi.org/10.1111/clr.13517
51. Scarano A, Orsini T, Di Carlo F, et al. (2021) Graphene-doped poly (methyl-methacrylate)(PMMA) implants: a micro-CT and histomorphometrical study in rabbits. *Int J Mol Sci* 22: 1441. https://doi.org/10.3390/ ijms22031441
52. Negri B, Calvo-Guirado JL, Pardo Zamora G, et al. (2012) Peri-implant bone reactions to immediate implants placed at different levels in relation to crestal bone. Part I: a pilot study in dogs. *Clin Oral Implants Res* 23: 228–235. https://doi.org/10.1111/j.1600-0501.2011.02158.x
53. Putri A, Pramanik F, Azhari A (2023) Micro computed tomography and immunohistochemistry analysis of dental implant osseointegration in animal experimental model: a scoping review. *Eur J Dent* 17: 623–628. https://doi.org/10.1055/s-0042-1757468
54. Zhi Q, Zhang Y, Wei J, et al. (2023) Cell responses to calcium- and protein-conditioned titanium: an in vitro study. *J Funct Biomater* 14: 253. https://doi.org/10.3390/jfb14050253
55. Scarano A, Tari Rexhep S, Leo L, et al. (2023) Wettability of implant surfaces: Blood vs autologous platelet liquid (APL). *J Mech Behav Biomed Mater* 126: 104773. https://doi.org/10.1016/j.jmbbm.2021.104773
56. Silva IR, Barreto ATS, Seixas RS, et al. (2023) Novel strategy for surface modification of titanium implants towards the improvement of osseointegration property and antibiotic local delivery. *Materials* 16: 2755. https://doi.org/10.3390/ma16072755
57. Van Oossterwyck H, Duyck J, Vander Sloten J, et al. (2000) Use of microfocus computerized tomography as a new technique for characterizing bone tissue around oral implants. *J Oral Implantol* 26: 5–12. https://doi.org/10.1563/1548-1336

AIMS Press